Design and Control of a Piezo Drill for Robotic Piezo-Driven Cell Penetration

Changsheng Dai, Liming Xin, Zhuoran Zhang, Guanqiao Shan, Tiancong Wang, Kaiwen Zhang, Xian Wang, Lap-Tak Chu, Changhai Ru, and Yu Sun

***Abstract*—Cell penetration is an indispensable step in many cell surgery tasks. Conventionally, cell penetration is achieved by passively indenting and eventually puncturing the cell membrane, during which undesired large cell deformation is induced. Piezo drills have been developed to penetrate cells with less deformation. However, existing piezo drills suffer from large lateral vibration or are incompatible with standard clinical setup. Furthermore, it is challenging to accurately determine the time instance of cell membrane puncturing; thus, the time delay to stop piezo pulsing causes cytoplasm stirring and cell damage. This letter reports a new robotic piezo-driven cell penetration technique, in which the piezo drill device induces small lateral vibrations and is fully compatible with standard clinical setup. Techniques based on corner-feature probabilistic data association filter and motion history images were developed to automatically detect cell membrane breakage by piezo drilling. Experiments on hamster oocytes confirmed that the system is capable of achieving a small cell deformation of 5.68 $\pm$ 2.74 μm (vs. 54.29 $\pm$ 10.21 μm by passive approach) during cell penetration. Automated detection of membrane breakage had a success rate of 95.0%, and the time delay between membrane breakage and piezo-vibration stoppage was 0.51 $\pm$ 0.27 s vs. 2.32 $\pm$ 0.98 s by manual stoppage of piezo pulsing. This reduced time delay together with smaller cell deformation led to higher oocyte post-penetration survival rate (92.5% vs. 77.5% by passive approach, n = 80 cells).**

***Index Terms*—Biological Cell Manipulation, Automation at Micro-Nano Scales, Cell Penetration, Piezo Drill.**

I. Introduction

CELL penetration is required in many cell surgery tasks, such as in vitro fertilization [1], mitochondrial disease treatment [2], and cloning [3]. To penetrate a cell, a sharp micropipette is used to passively indent and pierce the cell membrane. The penetration of mammalian oocytes (egg cells) is particularly challenging due to the surrounding zona pellucida, a protective layer made of glycoproteins [Fig. 1(a)]. Passive penetration of an oocyte unavoidably induces large deformations, as shown in Fig. 1(b).

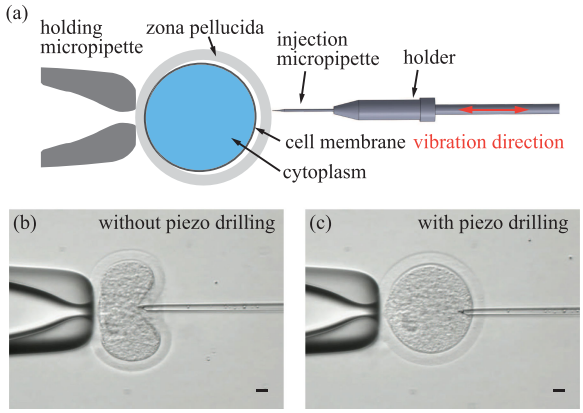

Fig. 1. (a) Piezo drill uses vibrations produced by a piezoelectric actuator to penetrate a cell. (b) Cell penetration without piezo drilling suffers from large cell deformation. (c) Cell penetration with piezo drilling induces less cell deformation. Scale bar: 10 μm.

Large deformations cause cell damage and lead to spindle (containing chromosomes) dislocation and development failure of mammalian oocytes [4]. Large deformations can also increase the internal pressure of the oocyte and contribute to oocyte degeneration. Smaller oocyte deformations are known to be instrumental for a higher fertilization rate and embryo development rate [5].

To reduce cell deformation during penetration, piezo drills were developed by using piezoelectric actuators to generate micropipette vibration [6]. The vibratory motions of the micropipette greatly facilitate cell penetration with less deformation, as shown in Fig. 1(c) and Supplementary Video. However, existing piezo drills suffer from large lateral vibration [7] and cause a larger area of damage on the cell membrane. To reduce the undesired lateral vibration, damping fluid (mercury [6] and Fluorinert [8]) are filled into the micropipette, but this remedy approach raises biosafety concerns. Although piezo drills were also developed to circumvent the use of damping fluid [9],

Manuscript received September 8, 2019; accepted November 29, 2019. Date of publication December 9, 2019; date of current version December 19, 2019. This letter was recommended for publication by Associate Editor S. Zuo and Editor P. Valdastri upon evaluation of the reviewers' comments. This work was supported by the Natural Sciences and Engineering Research Council of Canada (NSERC), the Canada Research Chairs Program, and the Ontario Research Fund – Research Excellence program. *(Corresponding authors: Liming Xin; Yu Sun.)*

C. Dai, Z. Zhang, G. Shan, T. Wang, K. Zhang, X. Wang, L.-T. Chu, and Y. Sun are with the Department of Mechanical and Industrial Engineering, University of Toronto, Toronto, ON M5S 3G8, Canada (e-mail: changsheng.dai@mail.utoronto.ca; zhuoran@mie.utoronto.ca; gq.shan@mail.utoronto.ca; tiancong.wang@mail.utoronto.ca; kw.zhang@mail.utoronto.ca; wangxiantju@hotmail.com; laptakchu8@gmail.com; sun@mie.utoronto.ca).

L. Xin is with the State Key Laboratory of Mechanical Transmissions, Chongqing University, Chongqing 400044, China (e-mail: xin_liming@hotmail.com).

C. Ru is with the Research Center of Robotics and Micro System and Collaborative Innovation Center of Suzhou Nano Science and Technology, Soochow University, Suzhou 215021, China (e-mail: rchhai@hotmail.com).

This article has supplementary downloadable material available at http://ieeexplore.ieee.org, provided by the authors.

Digital Object Identifier 10.1109/LRA.2019.2958734

piezoelectric actuators were placed concentrically behind the micropipette in these designs. Such designs alter the standard setup in clinics and biology labs, where the micropipette is mounted on a standard micropipette holder [see Fig. 1(a)]. A piezo drill that generates strong axial vibrations with small lateral vibrations and is compatible with a standard micropipette holder is desired.

Upon cell penetration, piezo pulsing needs to be stopped. Otherwise, micropipette vibration causes cytoplasm stirring and leads to poor cell development [10]. The time delay between manually identifying membrane breakage and stopping piezo pulsing is typically a few seconds. Minimizing this time delay demands the automation of piezo-driven cell penetration.

The detection of membrane breakage relies on identifying cell membrane's motion. When the indented cell membrane breaks, the tension on the elastic membrane is released, and the membrane recovers to its initial shape. For motion detection, background subtraction is commonly used by subtracting the stationary background to derive the foreground [11]. However, during cell penetration, besides the moving cell membrane, the micropipette in the background also moves. To cope with the moving background, foreground models can be learned from labeled data [12]; however, its performance degrades due to the unavoidable appearance change of cell membrane during penetration. Additionally, membrane breakage is identified by its backward motion, but the membrane also has forward motion generated by the indenting micropipette before breakage. Both micropipette motion and forward motion of the cell membrane must be excluded from membrane breakage detection.

To exclude the micropipette motion from membrane breakage detection, micropipette tracking is required. Tracking becomes challenging after the micropipette indents the cell since cell membrane and cytoplasm bring interferences and cause data association uncertainty. Nearest neighbor method is commonly used for data association by assigning the nearest measurement to the tracked object, but does not account for false association due to interferences [13]. Multiple hypothesis tracker uses the measurement history to estimate the object state but suffers exponential memory growth over time [14].

This letter reports a robotic piezo-driven cell penetration technique to effectively reduce cell deformation and damage. The challenges to overcome are as follows. (1) The piezo drill needs to be constrained on lateral vibration and be compatible with standard setup. (2) The tracking of micropipette during penetration is under interference from cell membrane and cytoplasm. (3) The time delay between cell membrane breakage and vibration stoppage should be minimized to reduce cell damage. To tackle these challenges, we developed an eccentric configuration with flexure beams for our piezo drill device, robust micropipette tracking, and automated detection of cell membrane breakage. Experimental results reveal that the system achieved cell deformation of 5.68 $\pm$ 2.74 μm, which was significantly less than the deformation of 54.29 $\pm$ 10.21 μm without piezo drilling. Micropipette tracking accuracy was 97.5%; the success rate of automated membrane breakage detection was 95.0%; and the time delay between cell membrane breakage and piezo-vibration stoppage was 0.51 $\pm$ 0.27 s (vs. 2.32 $\pm$ 0.98 s by manual operation).

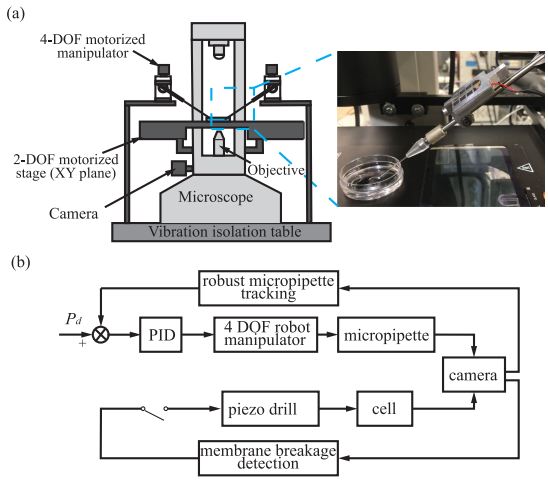

Fig. 2. (a) System setup. Inset shows the piezo drill device mounted on a standard micropipette holder. (b) System control architecture.

II. System Setup

As shown in Fig. 2(a), the system consists of an inverted microscope equipped with an X-Y motorized stage (H117, Prior). Micropipettes were mounted on two 4-DOF micromanipulators (MX7600, Siskiyou) with a motion resolution of 0.1 μm. A camera (scA1300-32 gm, Basler) was connected to the microscope to capture images at 30 frames per second. Inset of Fig. 2(a) shows the piezo drill mounted on a standard micropipette holder. To actuate the piezo drill, driving signals are generated by a custom-built circuit.

The control architecture of the robotic system is summarized in Fig. 2(b). Visual feedback of the micropipette is used to control the robotic manipulator for cell penetration. Based on membrane breakage detection, the piezo drill is stopped automatically to prevent disturbance to cytoplasm.

III. Piezo Drill Design

A. Mechanical Design and Analysis

Most of piezo drills adopted the concentric configuration in which the piezoelectric actuator is placed right behind the micropipette [9], [15]. Such a design disturbs the standard setup where a micropipette is mounted on a standard holder. Alternatively, eccentric configuration was developed to place the piezoelectric actuator beside the micropipette holder [6], [8]. In these devices, the piezoelectric actuator is connected to an inertial mass by a spring, and drives the vibration of the mass. However, it is difficult to keep vibration along the axial direction due to the lack of lateral constraints; therefore, these devices require the use of toxic damping fluid to reduce undesired lateral vibration.

Different from existing piezo drills, our design uses flexure beams to guide vibration along the axial direction and constrain

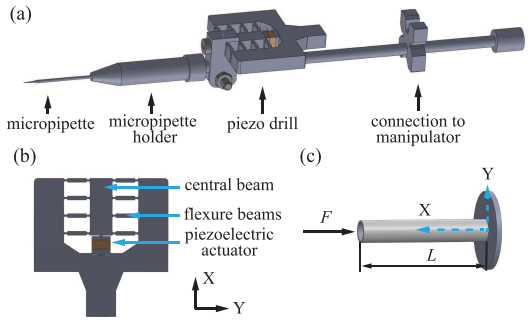

Fig. 3. (a) Eccentric configuration of piezo drill mounted on a standard micropipette holder. The eccentric configuration achieves compatibility with clinical setup. (b) Schematic of piezo drill design. Piezoelectric actuator is placed behind the central beam, and multiple pairs of flexure beams are connected to the central beam. The flexure beams are used to guide the motion of central beam along the penetration direction. (c) Dynamic models of the micropipette and holder.

lateral vibration. The piezo drill is eccentrically mounted beside a standard micropipette holder, which does not disturb standard clinical setup [Fig. 3(a)]. As shown in Fig. 3(b), the piezoelectric actuator is placed behind the central beam to drive its motion. Multiple pairs of flexure beams are connected to the central beam by flexure hinges. The flexure beams and hinges allow lower stiffness along the X axis (3.5 N/μm) than along the Y and Z axes (>200 N/μm). Thus, the vibration from the piezoelectric actuator is guided along the X axis (axial direction), resulting in small lateral vibration.

To prevent resonant vibration, dynamic models of micropipette holder and micropipette are established to determine their resonant frequencies, as shown in Fig. 3(c). According to the Euler-Bernoulli beam theory, the lateral motion of micropipette holder is

$$EI\frac{\partial^4 y}{\partial x^4} + F\frac{\partial^2 y}{\partial x^2} + \rho A\frac{\partial^2 y}{\partial t^2} + c\frac{\partial y}{\partial t} = 0 \tag{1}$$

where y is the lateral displacement of the micropipette holder; x is the position along the micropipette holder from its fixed position; E and I are elastic modulus and area moment of the micropipette holder, respectively; F is the axial force applied when penetrating a cell; ρ and A are the density and sectional area of the micropipette holder, respectively; and c is the viscous damping coefficient.

From (1) the resonant frequencies ω_n are

$$\omega_n = k_n^2\sqrt{\frac{EI}{\rho AL^4}} \tag{2}$$

where k_n is the wave number and is solved from the characteristic equation $1 + \cos k_n \cosh k_n = 0$.

Using the dynamic model, the resonant frequencies of glass micropipette are also determined. To derive the resonant frequencies of the piezo drill in Fig. 3(b), finite element analysis was performed. The resonant frequencies of micropipette, micropipette holder, piezo drill and the whole structure are summarized in Table I, which were used in the design of driving signals to prevent resonant vibration.

TABLE I
RESONANT FREQUENCIES OF PIEZO DRILL (KHZ)

Micropipette	Holder	Piezo drill	Whole structure
4.26	0.66	1.65	7.97
26.73	4.15	2.18	10.20
74.85	11.62	2.69	12.62
146.67	22.77	5.39	22.76
242.44	37.64	8.60	25.37

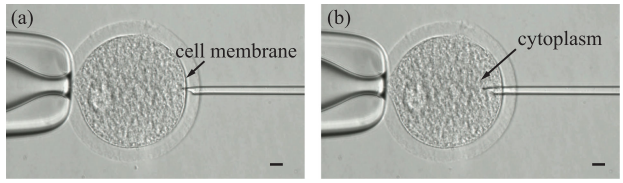

Fig. 4. (a) and (b) Micropipette tracking: interferences from cell membrane (a) and cytoplasm (b). The use of corner feature helps differentiate the micropipette from the interfering cell membrane and cytoplasm during cell penetration. Scale bar: 10 μm.

B. Driving Signal Design

The driving signal is used to actuate the piezoelectric actuator to induce micropipette vibration. It is a pulse wave, comprising multiple pulses with intervals among them. Comparing to continuous pulses without intervals, the pulse wave would transfer less power to the cell and reduce damage [7]. Since the frequency components of a pulse wave cover the full frequency spectrum, including the resonant frequencies determined in Section III-A, bandpass filter was designed to remove resonant frequency components from the driving signal. From Table I, the frequency range [13 kHz, 20 kHz] avoids all resonant frequencies. Thus, a fourth-order infinite impulse response filter with bandpass frequency of [13 kHz, 20 kHz] was designed as

$$y[n] = \sum_{k=0}^{4} b_k x[n-k] - \sum_{k=1}^{4} a_k y[n-k] \tag{3}$$

where y and x are the output and input of the filters, b_k and a_k are the kth feedforward and feedback coefficients.

IV. ROBOTIC PIEZO DRILLING

A. Robust Micropipette Tracking

To achieve robotic cell penetration, micropipette tracking is required to provide visual feedback. As discussed later, micropipette tracking is also used to exclude micropipette motion from membrane breakage detection. When the micropipette indents the cell, the cell membrane and cytoplasm interfere with micropipette tracking (see Fig. 4) and cause data association uncertainty. Most of tracking algorithms utilize the nearest neighbor method by associating the nearest measurement to the target, and cannot effectively deal with data association uncertainty [13]. Probabilistic data association filter (PDAF) is advantageous for tracking under interference because it performs measurement validation and uses the association probability of each valid measurement for state update [16].

The standard PDAF method only uses kinematics information (position and velocity), but during cell penetration, cell membrane and cytoplasm have similar position and velocity with the micropipette and can cause mismatch. Since the sharp micropipette has corner feature but cell membrane and cytoplasm lack, we formulated a corner-feature probabilistic data association filter to distinguish the micropipette from interferences. In the corner-feature PDAF method, the state vector of micropipette tip at time k is

$$X_k = [x\ y\ c\ \dot{x}\ \dot{y}\ \dot{c}]^T \tag{4}$$

where (x, y) is the position of the micropipette tip in the image frame, and c is the corner feature described as

$$c = det(\mathbf{M}) - k(trace(\mathbf{M}))^2 = \lambda_1\lambda_2 - k(\lambda_1 + \lambda_2)^2 \tag{5}$$

where λ_1, λ_2 are eigenvalues of $\mathbf{M}$. $\mathbf{M}$ is computed from image derivatives

$$\mathbf{M} = \sum_{x,y} w(x, y) \begin{bmatrix} I_x^2 & I_xI_y \\ I_xI_y & I_x^2 \end{bmatrix} \tag{6}$$

where I_x, I_y are image derivatives along x and y axes, respectively. $w(x, y)$ is the weight function.

Corner-feature PDAF calculates the Mahalanobis distance D_k between predicted measurement $\tilde{Z}_k = [\tilde{x}, \tilde{y}, \tilde{c}]^T$ and actual measurement $Z_k = [x, y, c]^T$ for measurement validation.

The association probability $P_k(i)$ determined by Mahalanobis distance are used to update the state vector X_k

$$X_k = \tilde{X}_k + G_k \sum_{i=1}^{N} P_k(i)[Z_k(i) - \tilde{Z}_k] \tag{7}$$

where G_k is filter gain. The inclusion of corner feature helps reduce data association uncertainty because when cell membrane or cytoplasm interferes with the micropipette tip, their difference in corner features contributes to a larger Mahalanobis distance and thus a smaller association probability.

B. Automated Detection of Membrane Breakage

After the cell membrane is penetrated, the piezo drill needs to be stopped to prevent stirring the cytoplasm and causing cell damage [10]. To minimize the time delay of stopping piezo drilling after membrane breakage, we developed a technique for automated detection of membrane breakage.

The detection of membrane breakage is intrinsically motion detection of the cell membrane. Upon breakage, the indented membrane elastically recovers towards its initial shape due to released tension. Background subtraction [11] is often used in motion detection by subtracting the stationary background to derive the moving foreground. However, there are two difficulties for the detection of membrane motion with this method. Besides the motion of the cell membrane, the micropipette tip also has motion during penetration, which cannot be excluded by background subtraction. Additionally, membrane breakage is identified by its backward motion, but the membrane also has forward motion generated by the indenting micropipette before breakage.

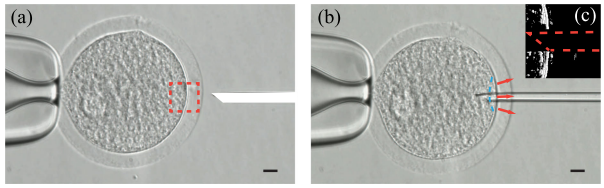

Fig. 5. (a) Region of interest shown as dashed box is determined around the penetration site. A mask is applied onto the micropipette to exclude its motion from membrane breakage detection. (b) After cell membrane breakage, the membrane has backward motion due to tension release, indicated by arrows. The dashed curve shows the membrane contour before breakage. (c) Motion history image is updated by gradient orientation to distinguish the backward motion of cell membrane. Dashed line shows the mask to exclude the micropipette motion. Scale bar: 10 μm.

To tackle these challenges, a region of interest (ROI) centered around the penetration site is firstly determined, as shown in Fig. 5(a). Within the ROI, the motion image is derived by taking the difference between two consecutive frames. To exclude micropipette motion from the membrane breakage detection, a mask is applied onto the micropipette [Fig. 5(a)]. The position (x_p, y_p) of the micropipette is obtained from robust micropipette tracking. Thus, the motion image of cell membrane is

$$M_{cm}(x, y, t) = M(x, y, t) - M_p(x_p, y_p, t) \tag{8}$$

where M, M_{cm}, and M_p are motion images of the ROI, cell membrane, and micropipette, respectively.

Motion history image (MHI) is used to enhance the membrane motion by accumulating the motion image M_{cm} over a period of time [17]. The motion image is binarized to construct motion history image as

$$H_\tau(x, y, t) = \begin{cases} \tau & \text{if } \Psi(M_{cm}(x, y, t)) = 1 \\ \max(0, H_\tau(x, y, t-1) - \gamma) & \text{otherwise} \end{cases} \tag{9}$$

where τ is the temporal extend of the movement, and γ is the decay parameter. Ψ is the binary image from the motion image M_{cm}.

To further distinguish the backward motion of the cell membrane after breakage [Fig. 5(b)], MHI is updated by keeping only those pixels with gradient orientation aligned with backward direction [see Fig. 5(c)], according to

$$\tilde{H}_\tau(x, y, t) = \begin{cases} 1 & \text{if } \left|\arctan(\frac{\partial H_\tau}{\partial y} / \frac{\partial H_\tau}{\partial x})\right| < \delta \text{ and } \frac{\partial H_\tau}{\partial x} > 0 \\ 0 & \text{otherwise} \end{cases} \tag{10}$$

where $\frac{\partial H_\tau}{\partial x}$, $\frac{\partial H_\tau}{\partial y}$ are spatial derivatives of H_τ over x and y axes, respectively. The update of MHI by gradient orientation helps reject the forward motion of cell membrane from membrane breakage detection.

With the visual feedback from robust micropipette tracking, the system controls the micropipette to reach the boundary of the oocyte and actuate the piezo drill. After membrane breakage is detected, the piezo drill is automatically stopped to prevent vibration-induced cytoplasm disturbance.

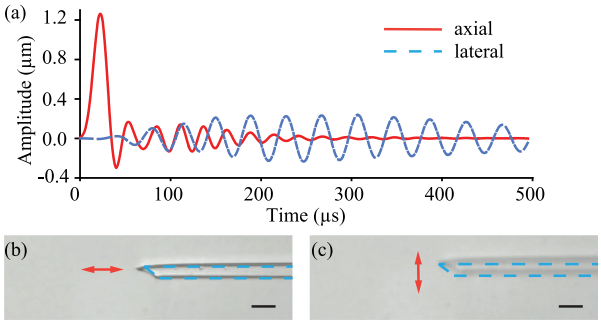

Fig. 6. (a) Finite element simulation: axial and lateral amplitudes of micropipette vibration. The piezo drill generates strong axial vibration and small lateral vibration. (b) and (c) Micropipette tip had smaller lateral vibration when driven with resonant frequencies removed (b) than without resonant frequencies removed (c). Arrows indicate the motion direction of the micropipette. The dashed line shows the micropipette contour when no driving signal was supplied. Scale bar: 10 μm.

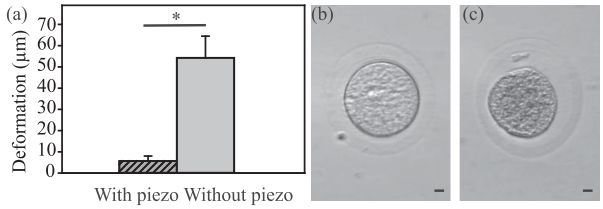

Fig. 7. (a) Cell deformation by piezo-driven penetration was significantly less than that without piezo drilling ($p < 0.05$, $n = 40$ for each group). (b) (c) Hamster oocytes were classified as (b) survived and (c) degenerated based on morphology criteria after incubation. Scale bar: 10 μm.

V. Results and Discussion

A. Piezo Drill Characterization

The piezo drill described here is the first eccentric, lateral-constrained device that is both compatible with clinical setup and free of damping fluid. In the design phase, finite element analysis was performed to quantify micropipette vibration produced by the piezo drill. In simulation the micropipette was surrounded by liquid (viscosity $\mu = 1.003$ mPa·s for cell culture medium). Mimicking the misalignment between the piezo actuator and micropipette in device assembly, a misalignment error of 5° was intentionally used in simulation. The driving signal was a 15 kHz pulse wave (peak voltage: 20 V; 20 pulses per second) filtered by [13 kHz, 20kHz] bandpass filter according to (3). The piezoelectric actuator generated an axial displacement of 0.8 μm and a lateral vibration of 0.08 μm. The vibration was transmitted to the micropipette tip, and maximum axial and lateral amplitudes of micropipette vibration were 1.25 μm and 0.23 μm, as shown in Fig. 6(a).

We also performed experimental characterization of micropipette vibrations. Videos were captured under 40× microscope objective at 30 Hz, and the boundaries of the blurred micropipette's contours were used to measure axial and lateral amplitudes (see Supplementary Video). Experimental measurements confirmed that the micropipette tip had a maximum axial and lateral vibration amplitude of 1.44 μm and 0.36 μm, respectively, with the same driving signal used in simulation (i.e., 15 kHz pulse wave, bandpass filtered) [Fig. 6(b)]. When the driving signal was not bandpass filtered, the micropipette tip's maximum axial and lateral vibration amplitudes were measured to be 1.26 μm and 1.80 μm, respectively [Fig. 6(c)]. The filter removes resonant frequencies from the driving signal, thus helps reduce the lateral vibration of the micropipette.

B. Piezo-Driven Cell Penetration

The system utilizes micropipette vibration to penetrate a cell membrane. The driving signal contains ten pulses per second to generate micropipette vibration. To quantitatively evaluate cell deformation and damage during penetration with and without piezo drilling, experiments were performed on 80 hamster oocytes. Cell deformation was measured as the maximum indentation of cell membrane before penetration. Cell deformation by piezo-driven penetration was measured to be 5.68 ± 2.74 μm, significantly less than the cell deformation of 54.29 ± 10.21 μm without piezo drilling ($p < 0.05$, $n = 40$ for each group), as shown in Fig. 7(a).

Cell damage was also compared between the two groups of oocytes that were penetrated with and without piezo drilling. After penetration, the oocytes were incubated for 12 hours and classified as survived or degenerated based on the standard morphology criteria reported in [18] [see Fig. 7(b) and (c)]. Those shrunk oocytes with condensed cytoplasm were regarded as degenerated. The oocytes penetrated with piezo drilling had a survival rate of 82.5% (33/40), which is higher than the survival rate of 77.5% (31/40) without piezo drilling. These results suggest penetration with our piezo drilling reduced cell damage during penetration. Note that in these experiments, cell membrane breakage detection and stoppage of piezo drilling were conducted manually. In order to further improve cell post-penetration survival rate by reducing the time delay between membrane breakage and piezo stoppage, we performed micropipette tracking and cell membrane breakage detection.

C. Robust Micropipette Tracking

Micropipette tracking is required for visual feedback and for excluding micropipette motion from membrane breakage detection. To tackle interferences from cell membrane and cytoplasm during penetration, we developed a corner-feature PDAF method to reduce data association uncertainty for robust micropipette tracking.

Tracking performance was quantitatively compared between the popular nearest neighbor method, standard PDAF, and corner-feature PDAF. The micropipette tip was continuously tracked during piezo-driven cell penetration of 40 oocytes. Success rate was quantified as

$$\text{success rate} = \frac{n_{\text{success}}}{n_{\text{success}} + n_{\text{mismatch}} + n_{\text{miss}}} \tag{11}$$

where n_{success} denotes the times of penetration when the tracking point was continuously on the micropipette tip; n_{mismatch} denotes the times when the tracking point was falsely assigned to the interfering cell membrane or cytoplasm; and n_{miss} denotes the

TABLE II
PERFORMANCE COMPARISON OF MICROPIPETTE TRACKING

Method	$n_{success}$	$n_{mismatch}$	n_{miss}	Success rate (%)
nearest neighbor	26	9	5	65.0
standard PDAF	33	6	1	82.5
corner-feature PDAF	39	1	0	97.5

times when the tracking point lost track of the moving micropipette tip.

The success rates of the nearest neighbor method, standard PDAF and developed corner-feature PDAF for micropipette tracking are summarized in Table II. The nearest neighbor method had a low success rate of 65.0% because it does not account for false association. The standard PDAF had a success rate of 82.5% since it only relies on kinematics information for object tracking. During penetration, the interfering cell membrane and cytoplasm had similar position and velocity with the micropipette, so it caused mismatch of the tracked micropipette using the standard PDAF method. The corner-feature PDAF method achieved a success rate of 97.5%, significantly higher than the nearest neighbor method and standard PDAF. The inclusion of the corner feature in (4) was effective in distinguishing the micropipette tip from interfering cell membrane and cytoplasm. The failure case was due to the attachment of mineral oil, used to cover cell culture medium to prevent evaporation, to the micropipette tip, which weakened the micropipette tip's corner feature.

D. Membrane Breakage Detection

After the cell is penetrated, the piezo drill needs to be stopped to prevent stirring cytoplasm and causing cell damage. In manual operation, it costs a few seconds for an experienced operator to identify membrane breakage and manually stop piezo drilling. To reduce this time delay, our system performed automated detection of membrane breakage. The membrane's backward motion after breakage was distinguished by gradient orientation in motion history images according to (10).

Automated detection of membrane breakage was evaluated in piezo-driven penetration of 40 hamster oocytes. The success rate of membrane breakage detection was 95.0%. For the few failure cases, the cell membrane broke once the micropipette contacted the membrane, and the membrane revealed very little backward motion. This can be attributed to the oocyte's poor mechanical characteristics [19].

We also quantified the time delay of piezo stoppage and cell damage. For 40 hamster oocytes, piezo drilling was stopped automatically after automated detection of membrane breakage. For another 40 hamster oocytes, membrane breakage detection and piezo stoppage were performed by two experienced operators. As shown in Fig. 8(a), automated detection of membrane breakage achieved a time delay of 0.51 ± 0.27 second, significantly less than the time delay of 2.32 ± 0.98 seconds by manual operation ($p < 0.05$, $n = 40$ for each group). The longer time

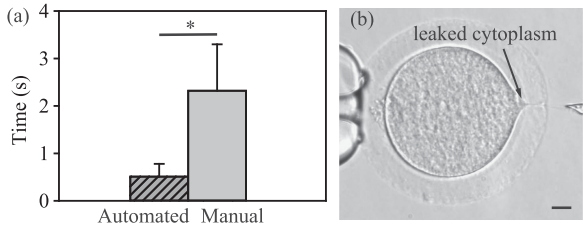

Fig. 8. (a) Time delay between membrane breakage and stoppage of piezo drilling was reduced significantly by automated detection of membrane breakage than by manual operation ($p < 0.05$, $n = 40$ for each group). (b) Cytoplasm leakage. Scale bar: 10 μm.

delay in manual operation undesirably lengthened vibration-induced stirring of the cytoplasm and caused cytoplasm leakage [see Fig. 8(b)].

After incubating the penetrated oocytes for 12 hours, we compared oocyte survival rates. When the piezo drill was automatically stopped, the oocytes had a survival rate of 92.5% ($n = 40$) vs. 82.5 % ($n = 40$) by manual membrane breakage detection and piezo stoppage. The survival rate of 92.5% was similar to the control group's survival rate of 95%, in which 40 hamster oocytes were directly cultured (without manipulation/penetration) for 12 hours. These results suggest that automated stoppage of piezo drilling was necessary and effective for reducing cell damage.

VI. CONCLUSION

This letter presented robotic piezo-driven cell penetration to reduce cell deformation and damage. The design of mechanical structure and driving signal of the piezo drill led to small lateral vibration and easy integration of the device into a standard setup. Cell deformation in penetration by piezo drilling was 5.68 ± 2.74 μm, significantly less than the deformation of 54.29 ± 10.21 μm without piezo drilling. Through robust micropipette tracking and membrane breakage detection, automated detection of cell membrane breakage achieved a success rate of 95.0%, and reduced the time delay of vibration stoppage after penetration from 2.32 ± 0.98 second in manual operation to 0.51 ± 0.27 second. The shorter time delay together with smaller cell deformation led to a higher oocyte survival rate of 92.5% (vs. 77.5% without piezo drilling).

REFERENCES

[1] P. Devroey and A. Van Steirteghem, "A review of ten years experience of ICSI," *Human Reproduction Update*, vol. 10, no. 1, pp. 19–28, 2004.
[2] A. Greenfield *et al.*, "Assisted reproductive technologies to prevent human mitochondrial disease transmission," *Nature Biotechnol.*, vol. 35, no. 11, p. 1059, 2017.
[3] Z. Liu *et al.*, "Cloning of macaque monkeys by somatic cell nuclear transfer," *Cell*, vol. 172, no. 4, pp. 881–887, 2018.
[4] Z. Luo *et al.*, "Deformation of a single mouse oocyte in a constricted microfluidic channel," *Microfluidics Nanofluidics*, vol. 19, no. 4, pp. 883–890, 2015.
[5] K. Yanagida *et al.*, "The usefulness of a piezo-micromanipulator in intracytoplasmic sperm injection in humans," *Human Reproduction*, vol. 14, no. 2, pp. 448–453, 1999.
[6] N. Yoshida and A. C. Perry, "Piezo-actuated mouse intracytoplasmic sperm injection ICSI," *Nature Protocols*, vol. 2, no. 2, p. 296, 2007.

[7] K. Ediz and N. Olgac, "Microdynamics of the piezo-driven pipettes in ICSI," *IEEE Trans. Biomed. Eng.*, vol. 51, no. 7, pp. 1262–1268, Jul. 2004.
[8] K. Hiraoka and S. Kitamura, "Clinical efficiency of piezo-ICSI using micropipettes with a wall thickness of 0.625 μm," *J. Assisted Reproduction Genetics*, vol. 32, no. 12, pp. 1827–1833, 2015.
[9] C. Ru *et al.*, "The development of piezo-driven tools for cellular piercing," *Appl. Sci.*, vol. 6, no. 11, p. 314, 2016.
[10] D. A. Fletcher and R. D. Mullins, "Cell mechanics and the cytoskeleton," *Nature*, vol. 463, no. 7280, p. 485, 2010.
[11] Y. Sheikh, O. Javed, and T. Kanade, "Background subtraction for freely moving cameras," in *Proc. IEEE Int. Conf. Comput. Vision*, 2009, pp. 1219–1225.
[12] P. Viola *et al.*, "Detecting pedestrians using patterns of motion and appearance," *Int. J. Comput. Vision*, vol. 63, no. 2, pp. 153–161, 2005.
[13] N. Chenouard *et al.*, "Objective comparison of particle tracking methods," *Nature Methods*, vol. 11, no. 3, p. 281, 2014.
[14] K. O. Arras, S. Grzonka, M. Luber, and W. Burgard, "Efficient people tracking in laser range data using a multi-hypothesis leg-tracker with adaptive occlusion probabilities," in *Proc. IEEE Int. Conf. Robot. Autom.*, 2008, pp. 1710–1715.
[15] W. Johnson *et al.*, "A flexure-guided piezo drill for penetrating the zona pellucida of mammalian oocytes," *IEEE Trans. Biomed. Eng.*, vol. 65, no. 3, pp. 678–686, Mar. 2018.
[16] Z. Zhang *et al.*, "Robotic immobilization of motile sperm for clinical intracytoplasmic sperm injection," *IEEE Trans. Biomed. Eng.*, vol. 66, no. 2, pp. 444–452, Feb. 2018.
[17] J. Liu *et al.*, "Robotic adherent cell injection for characterizing cell–cell communication," *IEEE Trans. Biomed. Eng.*, vol. 62, no. 1, pp. 119–125, Jan. 2015.
[18] J. Wu *et al.*, "Maturation and apoptosis of human oocytes in vitro are age-related," *Fertil. Steril.*, vol. 74, no. 6, pp. 1137–1141, 2000.
[19] G. D. Palermo *et al.*, "Oolemma characteristics in relation to survival and fertilization patterns of oocytes treated by intracytoplasmic sperm injection," *Human Reproduction*, vol. 11, no. 1, pp. 172–176, 1996.